Chemistry–A European Journal
Research Article
doi.org/10.1002/chem.202200949
Chemistry Europe
European Chemical Societies Publishing
www.chemeurj.org

Dissecting Noncovalent Interactions in Carboxyl-Functionalized Ionic Liquids Exhibiting Double and Single Hydrogens Bonds Between Ions of Like Charge

Lasse Hunger,[a] Loai Al-Sheakh,[a] Dzmitry H. Zaitsau,[a, b] Sergey P. Verevkin,[a, b] Andreas Appelhagen,[a] Alexander Villinger,[c] and Ralf Ludwig*[a, b, d]

Abstract: We show that the carboxyl-functionalized ionic liquid 1-(carboxymethyl)pyridinium bis(trifluoromethylsulfonyl)imide [HOOC-CH_2-py][NTf_2] exhibits three types of hydrogen bonding: the expected single hydrogen bonds between cation and anion, and, surprisingly, single and double hydrogen bonds between the cations, despite the repulsive Coulomb forces between the ions of like charge. Combining X-ray crystallography, differential scanning calorimetry, IR spectroscopy, thermodynamic methods and DFT calculations allows the analysis and characterization of all types of hydrogen bonding present in the solid, liquid and gaseous states of the ionic liquid (IL). We find doubly hydrogen bonded cationic dimers ($c^+{=}c^+$) in the crystalline phase. With increasing temperature, this binding motif opens in the liquid and is replaced by ($c^+{-}c^+{-}a^-$ species, with a remaining single cationic hydrogen bond and an additional hydrogen bond between cation and anion. We provide clear evidence that the IL evaporates as hydrogen-bonded ion pairs ($c^+{-}a^-$) into the gas phase. The measured transition enthalpies allow the noncovalent interactions to be dissected and the hydrogen bond strength between ions of like charge to be determined.

Introduction

Understanding and quantifying noncovalent interactions is a real challenge. A delicate balance between different types of interaction determines whether matter sticks together, gases condense into liquids, or liquids freeze into solids. This is in particular true for ionic liquids (ILs), which are attracting increasing interest in science and technology.[1–5] Their unique properties can be tailored for specific applications ranging from chemical synthesis and separation processes to media for electrochemical devices.[6–8] It is evident that a better understanding of their behavior at the microscopic scale will help to elucidate macroscopic fluid phenomena, and thus promote the industrial application. The suitable properties of these innovative fluids result from a mélange of Coulomb interactions, hydrogen bonding and dispersion forces. Designing these properties requires fundamental understanding of the strength, locality and directionality of the different types of interactions and how they contribute to the overall phase behavior.[9–12] In particular, local and directional hydrogen bonding has significant influence on IL behavior, leading to classification schemes based on the character of the doubly ionic hydrogen bonds.[13,14] In principle, two main types of hydrogen bonding are possible: one involving the Coulomb-enhanced interaction between a cation and an anion ($c^+{-}a^-$), and another occurring between ions of like-charge, which in the present case involves the positively charged cations ($c^+{-}c^+$).

One anticipates that the latter hydrogen bonds are significantly weakened by repulsive Coulomb forces, and the strengths of both types of H-bonds in ILs differ from the regular hydrogen bonds observed for neutral molecular clusters of water or alcohols.[15–18] In ILs, ($c^+{-}c^+$) hydrogen bonds might not appear to be important drivers of local structures because they have to compete with the repelling Coulomb forces between the cations as well as with the Coulomb enhanced ($c^+{-}a^-$) hydrogen bonds between cation and anion. Despite this expectation, however, structural motifs involving H-bonded cationic clusters were observed in the bulk liquid phase of hydroxy-functionalized ILs.[19–32] In particular, FTIR measurements in the pure ILs clearly showed two distinct vibrational

[a] L. Hunger, L. Al-Sheakh, Dr. D. H. Zaitsau, Prof. Dr. S. P. Verevkin, A. Appelhagen, Prof. Dr. R. Ludwig
Institut für Chemie, Abteilung für Physikalische Chemie
Universität Rostock
Albert-Einstein-Str. 27, 18059 Rostock (Germany)
E-mail: ralf.ludwig@uni-rostock.de
[b] Dr. D. H. Zaitsau, Prof. Dr. S. P. Verevkin, Prof. Dr. R. Ludwig
Department LL&M, University of Rostock
Albert-Einstein-Str. 25, 18059 Rostock (Germany)
[c] Dr. A. Villinger
Institut für Chemie, Abteilung für Anorganische Chemie
Universität Rostock
Albert-Einstein-Str. 3a, 18059 Rostock (Germany)
[d] Prof. Dr. R. Ludwig
Leibniz-Institut für Katalyse an der Universität Rostock e.V.
Albert-Einstein-Str. 29a, 18059 Rostock (Germany)

Supporting information for this article is available on the WWW under https://doi.org/10.1002/chem.202200949
Part of a Special Collection on Noncovalent Interactions.

bands that are assigned to (c^+–a^-) and (c^+–c^+) hydrogen bonded species. It is worth noting that the (c^+–c^+) hydrogen bonds are evidently stronger than those in the (c^+–a^-) case as indicated by the magnitudes of the redshifts of their corresponding vibrational bands.[19–22] We systematically showed how these three molecular ion parameters support like-charge attraction. The use of polarizable cations, weakly interacting anions, and long alkyl chains results in (c^+–c^+) clustering already at room temperature. Moreover, we demonstrated that micro structuring affects macroscopic behavior of this type of ILs. We observed that substantial (c^+–c^+) interaction prevents ILs from crystallizing. Instead, these ILs supercool and finally form a glass.[23]

For hydroxy-functionalized ILs also positively charged clusters were observed by means of CIVP spectroscopy.[33–36] Supported by double resonance techniques, Menges et al. showed that for the IL 1-(2-hydroxyethyl)-3-methylimidazolium bis(trifluoromethylsulfonyl)imide (or ($HEMIm^+$)(NTf_2^-)) the two cations are linked through hydrogen bonding while one OH is attached to an oxygen of the anion resulting in positively charged ($HEMIm^+$)$_2$(NTf_2^-)$_1$ clusters of type (c^+–c^+–a^-).[33] In larger complexes ($HEMIm^+$)$_3$(NTf_2^-)$_2$ even contact between three cations was detected in (c^+–c^+–c^+–a^-)(a^-) isomers.[34] However, the counterions still play a crucial role for the stability of the singly charged (2,1) and (3,2) complexes as shown by accompanying quantum chemical calculations.[35–41] These studies showed that for investigating singly or doubly charged cationic clusters in more detail a consideration of stronger H-bonding between the ions of like-charge is required. The H-bond strength even in larger, cooperatively bound cationic clusters of hydroxy-functionalized ILs is not sufficiently strong to achieve this goal.[37–41]

It is the purpose of this work to realize this idea by using carboxyl-functionalized ionic liquids. Two strong hydrogen bonds (HB) between the cations, denoted as (c^+=c^+), mimic the HB motif of formic acid, the archetype of double hydrogen bridges (Scheme 1). The strongly enhanced HB interaction is supposed to overcome the repulsive Coulomb forces between the cations supporting the concept of anti-electrostatic hydrogen bonding.[42–45] This very productive cation–cation motif with two carboxyl groups engaged in antiparallel bridging H-bonds should benefit from the powerful cooperativity of coupled donor–acceptor interactions. After providing a new synthesis route for having larger, purified amounts of the sample, we developed a combined experimental and theoretical approach for studying and quantifying all types (Scheme 2) of hydrogen bonding (c^+–a^-), (c^+–c^+) and (c^+=c^+) possibly present in the solid, liquid and gaseous states of the IL. We determine the crystalline structure by X-ray diffraction observing the double hydrogen bond motif solely. Upon melting, the ring motif of the doubly hydrogen bonded cations (c^+=c^+) opens and is replaced by HB complexes (c^+–c^+–a^-) with one remaining HB (c^+–c^+) and an additional HB (c^+–a^-) between cation and anion. This transition between these HB motifs, we recorded by IR spectroscopy in the transmission and/or the attenuated total reflection (ATR) modes as a function of temperature. Reliable estimates of the vaporization enthalpies and DFT calculated complexes, which represent the characteristic features of the different types of HBs, allow the determination of the transition enthalpies and finally the quantification of the differently strong hydrogen bonds. For comparison, we applied the same approach on phenyl-acetic acid, wherein the molecules mimic the cationic structure present in the ionic liquid (Scheme 1). That allows the HB strength of the molecular dimers (m=m) to be related to cationic dimers (c^+=c^+) in ILs. Our methodology toolbox provides detailed insight into the nature of non-covalent interaction of ionic liquids.

Strategy of this study and investigated complexes

We analyzed differently hydrogen bonded complexes supposed to be present in the solid, liquid or in the gaseous phases of the ionic liquid 1-(carboxymethyl)pyridinium bis(trifluoromethylsulfonyl)imide [HOOC-CH_2-py][NTf_2] (Scheme 1). For the neutral complexes (HOOC-CH_2-py^+)$_2$(NTf_2^-])$_2$, three types of hydrogen bonding motifs might be formed as shown in Scheme 2:

a) Two cations HOOC-CH_2-py^+ are doubly hydrogen bonded with each other and two anions are attached to the cations without specific interaction, giving complex (c^+=c^+)(a^-)$_2$.
b) In a (c^+–c^+–a^-)(a^-) complex, the OH group on one cation HOOC-CH_2-py^+ binds to the carbonyl group CO on the other, while the OH group of the other attaches an oxygen atom of the anion.
c) Both cations form single hydrogen bonds to one of the anions without any hydrogen bond formed among them, denoted as (c^+–a^-)$_2$.

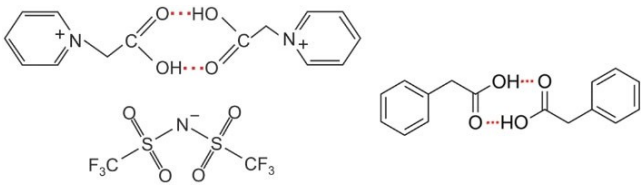

Scheme 1. Structural motif of the doubly hydrogen bonded cationic dimer [HOOC-CH_2-py^+]$_2$ possibly formed in the ionic liquid [HOOC-CH_2-py][NTf_2] in the presence the weakly interacting anions bis(trifluoromethylsulfonyl)imide [NTf_2^-] (left). Structural motif of the doubly hydrogen bonded dimer of phenyl-acetic acid, wherein the molecules mimic the cationic structure present in the IL (right).

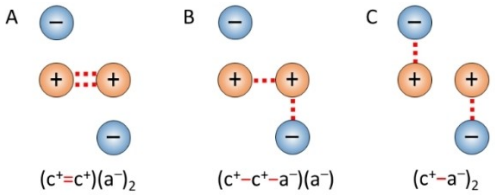

Scheme 2. Illustration of competing interactions at play in the ionic liquids [HOOC-CH_2-py][NTf_2] comprising (c^+=c^+)(a^-)$_2$, (c^+–c^+–a^-)(a^-) and (c^+–a^-)$_2$ complexes.

Experimental Section

Synthesis and characterization

The synthesis of the ionic liquid 1-(carboxymethyl)pyridinium bis(trifluoromethylsulfonyl)imide [HOOC-CH_2-py][NTf_2] via the 1-(carboxymethyl)pyridinium chloride [HOOC-CH_2-py][Cl] has been already reported in the literature.[46] Therein, a metathesis reaction was used to exchange the chloride anion for a bis(trifluoromethylsulfonyl)imide anion, starting from the commercially available 1-(carboxymethyl)pyridinium hydrochloride. The IL has a melting point at 32 °C. With this synthetic route, we could only collect a few single crystals for structure determination. However, we had to recognize that the resulting product included irremovable impurities, and the ionic liquid was not usable for other experiments. Consequently, we developed a new synthesis route (Scheme 3). In short: we synthesized the IL in two reaction steps. In the first step, we prepared the 1-(carboxymethyl)pyridinium bromide as follows:

We dissolved pyridine (189.63 mmol) in 100 mL of acetonitrile and added the mixture dropwise to a solid 2-bromoacetic acid within an hour with vigorous stirring at 278 K. The resulting crystalline compound we filtered, washed several times with acetonitrile and acetone, dried under vacuum at 333 K and kept under argon for the next step.

The second stage is the metathesis reaction. Equimolar amounts of lithium bis(trifluoromethanesulfonyl)imide and 1-(carboxymethyl)pyridinium bromide are dissolved in water, resulting an upper aqueous and a lower organic layer. The latter includes the 1-(carboxymethyl)pyridinium bis(trifluoromethylsulfonyl)imide product and trace amounts of lithium bromide, which has been removed by washing several times. The residual amount of the Br anion was determined using the reaction with silver nitrate. Finally, we dried the sample under vacuum at 333 K. Karl-Fischer titration showed that the water content below 100 ppm.

The single crystal of the ionic liquid 1-(carboxymethyl)pyridinium bis(trifluoromethylsulfonyl)imide [HOOC-CH_2-py][NTf_2] with approximate size and quality was suited for structure analysis by X-ray. The X-ray quality crystal was selected in Fomblin YR-1800 perfluoroether at ambient temperature. The sample was cooled to 123(3) K during measurement. The data were collected on a Bruker KAPPA APEX II diffractometer using $Mo_{K\alpha}$ radiation ($\lambda = 0.71073$). The structures were solved by direct methods (*SHELXS-2013*) and refined by full-matrix least squares procedures (*SHELXL-2013*).[47] Semi-empirical absorption corrections were applied (*SADABS*).[48] All non-hydrogen atoms were refined anisotropically, hydrogen atoms were included in the refinement at calculated positions using a riding model.

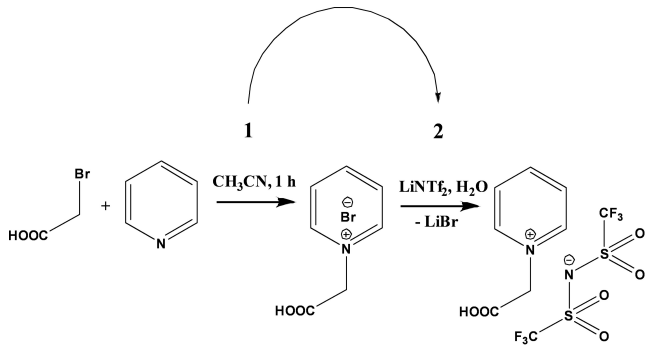

Scheme 3. Reaction scheme for the synthesis of the ionic liquid 1-(carboxymethyl)pyridinium bis(trifluoromethylsulfonyl)imide [HOOC-CH_2-py][NTf_2].

Deposition Number 2178447 contains the supplementary crystallographic data for this paper. These data are provided free of charge by the joint Cambridge Crystallographic Data Centre and Fachinformationszentrum Karlsruhe Access Structures service.

The thermal behavior of [HOOC-CH_2-py][NTf_2] was studied with Mettler Toledo DSC 823e coupled with Huber TC125MT cooler. The sample was placed in the standard non-pinned aluminium pan of 40 μL volume. All handling operations with sample were carried out in glove-box under nitrogen atmosphere (residual concentrations of oxygen 1.0 ppm and water 0.3 ppm). Pans and samples were weighted with Sartorius MSE3.6P-000-DM microbalances with the standard uncertainty of 5×10^{-6} g. The calibration of Mettler Toledo DSC 822e was checked with melting behavior of the reference indium sample. The temperature of fusion agreed with recommended value better than 0.5 K.

The temperature profile of the DSC run was as follows: cooling down to 173 K at 10, 5 or 1 K·min^{-1} rates and keeping for annealing for 15 minutes at this temperature. After that the sample was heated up to 323 K with heating rates of 1, 5 or 10 K·min^{-1}. The DSC studies of the thermal behavior of [HOOC-CH_2-py][NTf_2] were repeated twice with the samples of the same batch. The DSC charts and the summary on phase transition are given in the Supporting Information).

Transmission FTIR and attenuated total reflection (ATR) spectroscopy

Mid infrared (MIR) measurements of the IL 1-(carboxymethyl)pyridinium bis(trifluoromethylsulfonyl)imide [HOOC-CH_2-py][NTf_2] were performed with a Bruker Tensor II FTIR spectrometer. An L.O.T.-Oriel variable-temperature cell equipped with CaF_2 windows having a path length of 12 μm was used for the variable-temperature experiments between 193 and 413 K in steps of 20 K. The cell is cooled using a liquid ethanol/nitrogen mixture. For each spectrum 128 scans were recorded at a spectral resolution of 1 cm^{-1}.[49]

Infrared spectra of phenyl-acetic acid were recorded from 293 to 343 K in the solid and from 363 to 473 K in steps of 10 K on a Bruker Vector 22 FTIR spectrometer with a Globar® IR source, KBr beam splitter and a DTGS detector. The FTIR spectrometer was equipped with a MKII Golden Gate™ single reflection ATR system and a Golden Gate™ heated diamond crystal 45° ATR top plate with a 3000 Series™ High Stability Temperate Controller and a Golden Gate™ Reactive Sample Anvil from SPECAC.

The spectra were recorded with the OPUS 6.5 spectroscopy software from BRUKER in the spectral range between 4500 to 600 cm^{-1} with a resolution of 2 cm^{-1} and 128 scans. The aperture setting was 3 mm and the scanner velocity was 7.5 kHz. The Mertz phase correction and Blackman-Harris (3-Term) apodization function were employed. Atmospheric compensation and baseline correction were performed with the OPUS 6.5 spectroscopy software.

The IR spectra were deconvoluted separately into a number of Voigt profiles (convolution of Lorentzian and Gaussian functions) following the Levenberg-Marquardt procedure. The Voigt profiles have four parameters: maximum intensity, frequency, half-width of the Lorentzian, and half-width of the Gaussian. The software used for spectral deconvolution was developed by Dr. Henning Schröder from the Institute of Mathematics at the University of Rostock and

is intended for the use with the MATLAB® software package by MathWorks®.

Density functional theory (DFT) calculations of neutral clusters

We calculated neutral clusters including up to twelve ion pairs (n = 2, 4, 6, 8, 10, 12) at the B3LYP/6-31G* level of theory.[50] The widely popular hybrid density functional B3LYP is known to lack a proper description of dispersion. Thus, we re-optimized all clusters at the B3LYP–D3/6-31G* level of theory considering additional dispersion interaction as provided by Grimme's D3 method.[51–53] For calculating all clusters up to n = 12 at the same level of theory, we had to use the small 6–31G* basis set. It includes polarization functions and has been shown to be suitable for calculating hydrogen-bonded clusters.[54–57] Heavily questioned recently, counterpoise (CP) correction has not been applied.[58–60] Intrinsic CP artifacts for ion pair clusters add to fundamental concerns that this procedure is generally unreliable for correcting basis set superposition error (BSSE).[59] Nevertheless, that CP correction to the calculated dimers play a minor role of the BSSE correction for the resulting structures and energies.[61]

We calculated differently hydrogen bonded complexes exhibiting exclusively $(c^+{=}c^+)(a^-)^2$, $(c^+{-}c^+{-}a^-)(a^-)$, and $(c^+{-}a^-)^2$ structural motifs. In Figure 1. these complexes are shown for n = 2: a) two cations are doubly hydrogen bonded and two anions are attached to the cations without specific interaction $(c^+{=}c^+)(a^-)_2$; b) the OH group on one cation binds to the carboxyl group CO on the other, while the OH group of the other attaches an oxygen atom of the anion resulting in a $(c^+{-}c^+{-}a^-)(a^-)$ complex; c) both cations form single hydrogen bonds with two anions in two complexes $(c^+{-}a^-)^2$.

For reliable comparison of the binding energies in the $(c^+{=}c^+)(a^-)^2$ complexes with those in the other hydrogen bonded complexes $(c^+{-}c^+{-}a^-)(a^-)$ and $(c^+{-}a^-)$, we had to focus on even numbers for n. This means that for n = 4 we have twice as many and for n = 12 six times as many of these structural motives present in the clusters.

Results and Discussion

The solid phase: Crystal structure reveals ($c^+{=}c^+$) cationic dimers

The carboxyl-functionalized ionic liquid [HOOC-CH_2-py][NTf_2] prepared in this work has a melting point of about 305 K and it was crystallized as a fine needles suitable for the X-ray study. The X-ray structure shows the characteristic double hydrogen bonding motif between the two carboxyl groups of the cations, whereas the two weakly interacting bis(trifluoromethylsulfonyl)imide anions are attached but not involved in hydrogen bonding with any of the cations as shown in Figure 2. This structural motif as known for formic acid, the archetype of double hydrogen bridges, is characterized by two strong hydrogen bonds indicated by two short and almost similar R(O···O) distances between the hydroxy oxygen and the carbonyl oxygen of about R(O2···O3) = 2.633 Å and R(O1···O4) = 2.636 Å, respectively (Figure 2). Obviously, the two strong hydrogen bonds overcome the repulsive Coulomb forces between the carboxyl-functionalized cations and successfully compete with hydrogen bonding between cation and anion, although the latter is enhanced by attractive Coulomb interaction. For simple hydroxy-functionalized ionic liquids we showed earlier that strong cationic cluster formation prevents crystallization resulting in supercooled and finally glassy systems, whereas weak cationic cluster formation completely disappears in the solid state and only hydrogen bonding between cation and anion remains.[26,31] This is not the case in the solid [HOOC-CH_2-py][NTf_2], where two strong hydrogen bonds in the motif ($c^+{=}c^+$) are obviously stronger than the possible single cation–cation ($c^+{-}c^+$) and cation–anion ($c^+{-}a^-$) hydrogen bonds between the molecular ions. In the nearest future, we plan to investigate by IR and NMR spectroscopy a series of ionic liquids [HOOC-$(CH_2)_n$-py][NTf_2], where the carboxyl group gradually distance from the cation. We are interested whether the ($c^+{=}c^+$) HB bond motif survives the phase transition from the solid to the liquid phase and whether it remains stable with increasing temperature. Synthesis of ILs [HOOC-$(CH_2)_n$-py][NTf_2] with n > 1 for decreasing Coulomb repulsion due to methylene group spacers and increasing the HB strength at the same time is in progress in our lab.

The occurrence of strong like-charge attraction already in the solid state raises the question whether the characteristic H-

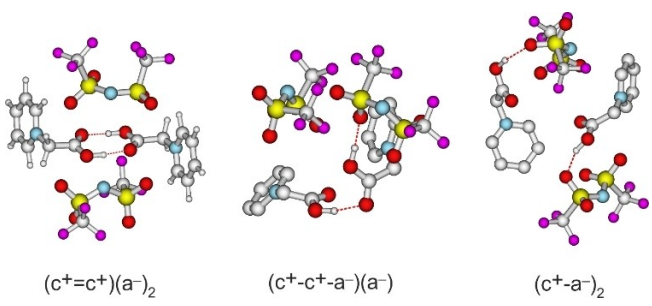

Figure 1. Calculated hydrogen bonded complexes $(c^+{=}c^+)(a^-)_2$, $(c^+{-}c^+{-}a^-)(a^-)$ and $(c^+{-}a^-)_2$ as possible constituents in the ionic liquids [HOOC-CH_2-py][NTf_2].

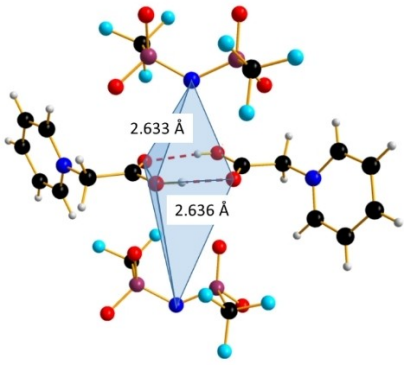

Figure 2. Solid-state structure of the ionic liquid 1-(carboxymethyl)pyridinium bis(trifluoromethylsulfonyl)imide [HOOC-CH_2-py][NTf_2]. The X-ray structure shows the favorable double H-bond motif formed between the carboxyl-functionalized cations, whereas the weakly interacting anions are not involved in hydrogen bonding, sitting above and below this structural motif. The hydrogen bonds are denoted by dashed lines.

bond motif will survive, if the counterions are removed successively, leading to singly charged cationic complexes $(HOOC\text{-}(CH_2)_n\text{-}py^+)_2(NTf_2^-)$ and finally pure cationic complexes $(HOOC\text{-}(CH_2)_n\text{-}py^+)_2$.

The liquid phase: Transition from $(c^+{=}c^+)(a^-)^2$ to $(c^+{-}c^+{-}a^-)(a^-)$ hydrogen bonds observed by IR spectroscopy

We measured the IR absorption spectra of 1-(carboxymethyl)pyridinium bis(trifluoromethylsulfonyl)imide for a broad range of temperatures between 193 and 413 K in 20 K steps. It has turned out that this IL can be undercooled and measured below the melting point of 305 K and glass transition temperature at about $T_g = 243$ K (see DSC thermograms in the Supporting Information). Although covering wavenumbers between 600 and 4500 cm^{-1}, we mainly focus on the C=O stretching vibrational bands which are usually observed between 1600 and 1800 cm^{-1}. These C=O bands are sensitive probes of hydrogen bonding and shift to lower wavenumbers with increasing strength of the hydrogen bonds. As shown above, the X-ray diffraction pattern of the crystalline IL has proven the existence of cationic dimers, which are characterized by two strong hydrogen bonds between the hydroxy H-bond donor position and the carbonyl H-bond acceptor position of the carboxyl functional groups of either cation. This binding motif is typically reflected in the solid state ATR IR spectra showing symmetric and asymmetric C=O stretch vibrational bands separated by about 50 cm^{-1} in the calculated cyclic dimer. Due to the significantly larger transition dipole moment, most of the intensity is focused in the asymmetric C=O stretching band. We clearly observed that the most intense band at 1753 cm^{-1} assigned to the asymmetric stretch of the C=O bond within the cyclic dimer ($^+c{=}^+c$; here I_4) is decreasing with increasing temperature to the benefit of a new vibrational band occurring at 1779 cm^{-1} (here I_5). The latter vibrational frequency is referred to an almost freely vibrating C=O bond in the overall environment of the IL (Figure 3). Obviously, increasing temperature breaks one of the hydrogen bonds of the cyclic dimers. For better understanding of the temperature behavior in the liquid phase, we deconvoluted the IR spectra simultaneously with temperature. We used three vibrational bands for describing the measured spectra for all temperatures. The vibrational bands I_1 and I_2 with maxima at 1634 and 1640 cm^{-1} were not considered here, because they are not directly related to the C=O stretches. They describe the C–N vibrational bands of the pyridinium ring system of the cations. The deconvoluted spectra in the C=O stretching region is shown in Figure 4 for temperatures 253, 293, 353 and 413 K, respectively. We observed that the bands I_3 and I_4 decrease to the benefit of band I_5. Thus, the temperature-dependent behavior describes the transition from the doubly H-bonded cyclic dimers ($c^+{=}c^+$) and the singly H-bonded linear cationic dimer ($c^+{-}c^+{-}a^-$) with one additional H-bond to an oxygen of the NTf_2 anion. We calculated the equilibrium constants K for both species from the ratios of the IR intensities I_4 and I_5. In Figure 5a, we show the resulting linear plot of $\ln K$ versus $1000/T$ indicating van 't Hoff behavior. From the slope we derive the transition enthalpy $\Delta H_{trans} = -8.0$ kJ mol^{-1}, which is released by breaking one of hydrogen bonds in the cyclic cationic dimers. For completeness we also show the temperature behavior of the equilibrium constants $K = (I_3 + I_4)/I_5$, wherein the vibrational band I_3 (also related to the cyclic dimers) with minor intensity is taken into account as well (Figure 5b). The resulting transition enthalpy $\Delta H_{trans} = -8.2$ kJ mol^{-1} is only slightly different from the other value, indicating that we addressed the same transition in both cases. These values are less than half of the typical H-bond energy, which is in the order of 20 kJ mol^{-1}.[15–18] This means that the strong H-bonds in the cationic dimers are partially counterbalanced by the repulsive Coulomb forces, resulting in significantly smaller HB energies than known for the same structural motifs in molecular systems such as formic or acidic acid.[62–64]

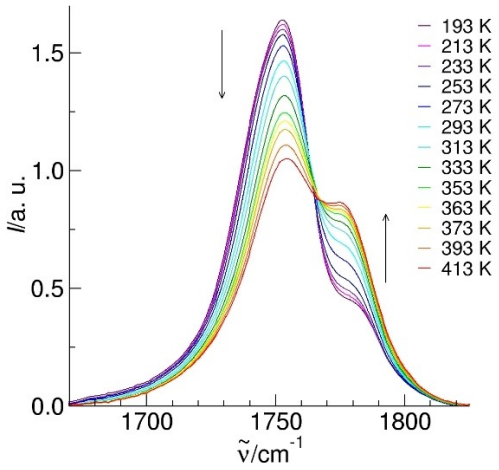

Figure 3. Temperature-dependent IR spectra in the C=O stretching region ranging from 193 to 413 K. In the liquid spectra, we observe the vibrational bands of the doubly H-bonded cationic dimer ($c^+{=}c^+$) around 1755 cm^{-1}, and that of the singly H-bonded cationic dimers in ($c^+{-}c^+{-}a^-$) complexes at about 1780 cm^{-1}. With increasing temperature the intensities of the ($c^+{=}c^+$) complexes decrease in favor of the intensities of the ($c^+{-}c^+{-}a^-$) complexes, as indicated by the arrows.

For a more reliable comparison between hydrogen bonded cationic and molecular dimers, we measured the IR spectra of phenyl-acetic acid (PAA) between 293 and 473 K in 10 K steps (Figure 6). The PAA molecule is the molecular mimic of the 1-(carboxymethyl)pyridinium cation as present in the IL. Up to the melting point at around 353 K, the spectra show the typical symmetric and asymmetric C=O stretch vibrational bands with dominant intensities for the asymmetric contribution. Upon melting, the cyclic HB motif mainly survives and only minor ring opening is observed. At the same time, the maxima of the bands shift from 1689 cm^{-1} at 293 K to 1705 cm^{-1} at 363 K indicating weakening of the HBs in the cationic dimers as reflected in the melting enthalpies of about 17 ± 5 kJ mol^{-1} shown in the DSC thermograms (see the Supporting Information).

With increasing temperature from 353 to 473 K, the formation of linear dimers in PAA increases at the expense of

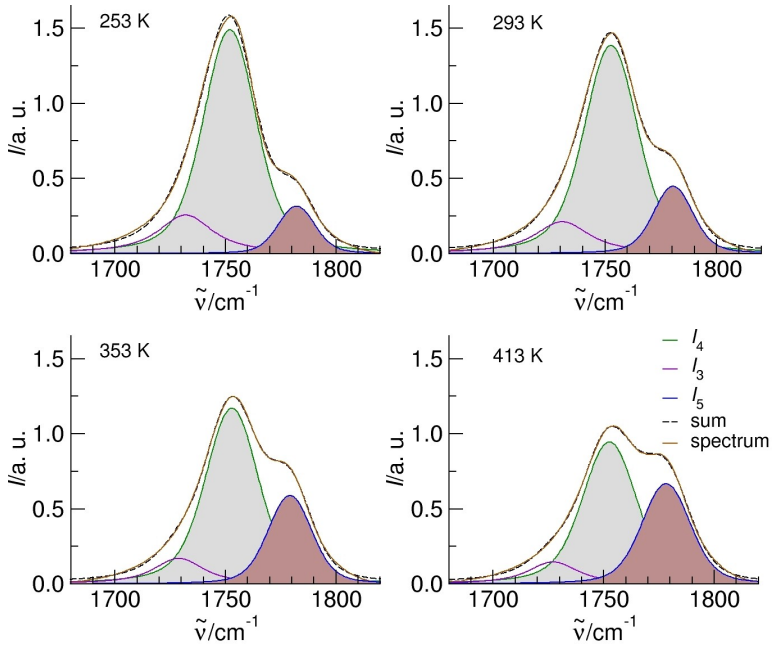

Figure 4. Deconvoluted IR spectra in the C=O stretching region of the IL at temperatures 253, 293, 353 and 413 K. The intensities of the vibrational bands I_3 and I_4 decrease to the benefit of that of I_5.

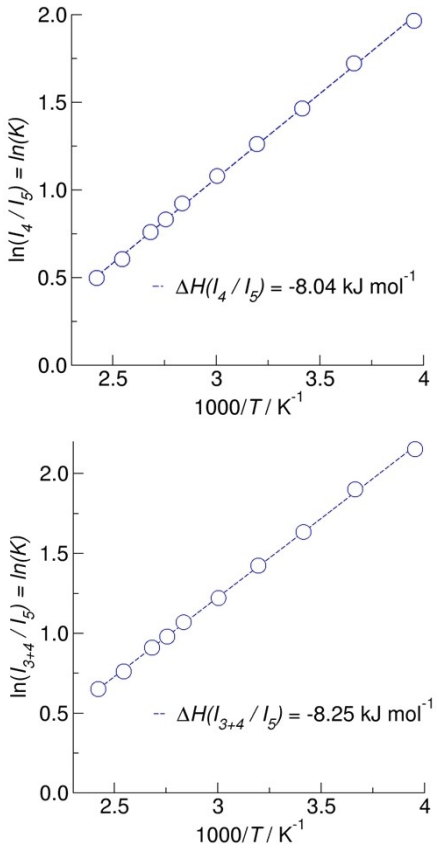

Figure 5. Plots of the natural logarithm of the ratios a) I_4/I_5 and b) I_{3+4}/I_5 versus inverse temperature taken from the deconvoluted spectra in Figure 6 between 253 and 413 K. The dashed lines represent linear fits ($R^2 \geq 0.99$) with slopes indicating the transfer enthalpies.

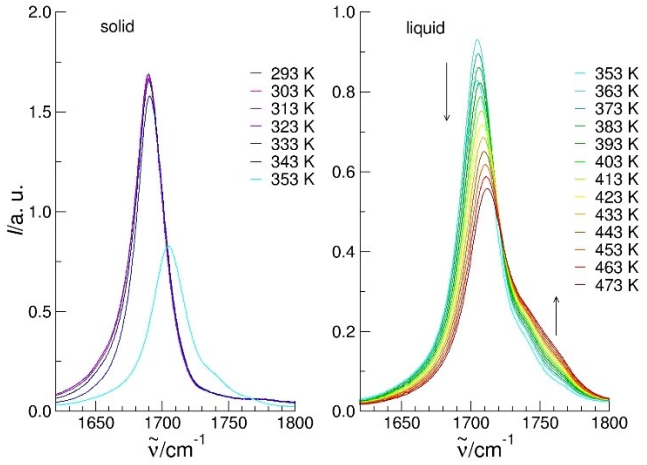

Figure 6. Temperature-dependent ATR-IR spectra of the C=O stretching region for phenylacetic acid (PAA). In the solid state, spectra between 293 and 343 K are characterized by almost temperature-independent frequencies of the cyclic dimers. The first liquid spectrum at 353 K, just above the melting point, shows an additional vibrational band of a non-hydrogen-bonded C=O, thus indicating linear, singly H-bonded dimers. In the liquid spectra from 353 to 473 K, contributions from the cyclic dimer decrease with increasing temperature, and contributions from the linear dimer increase with increasing temperature. The arrows at different spectral positions indicate the changes in intensity with increasing temperature.

cyclic dimers in the liquid phase, finally yielding the energy of the released hydrogen bond as illustrated in Figure 7. We calculated the equilibrium constants K for both species from the ratios of the IR intensities I_4 and I_5. In Figure 8, we show the resulting linear plot of $\ln K$ versus 1000 K/T indicating van 't Hoff behavior. From the slope we derive the transition enthalpy $\Delta H_{trans} = -17.4\ kJ\,mol^{-1}$. Compared the cationic dimers, the

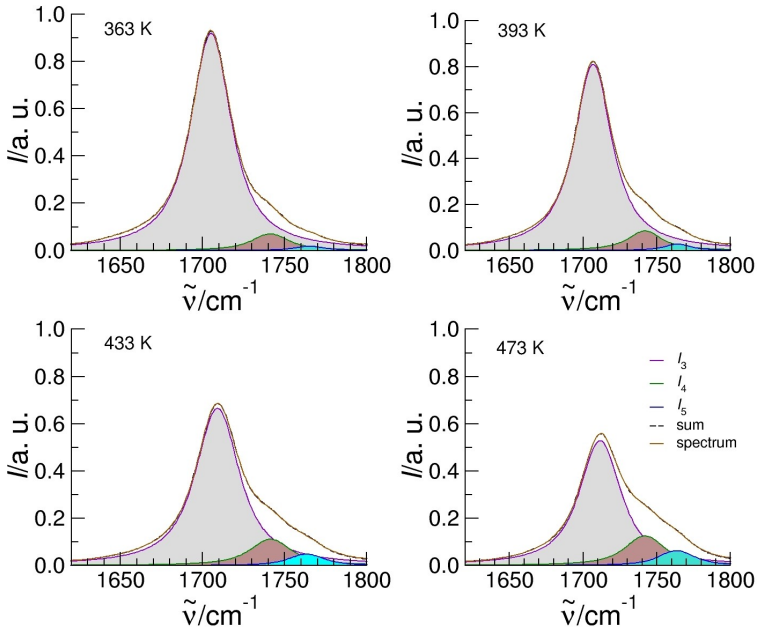

Figure 7. Deconvoluted ATR-IR spectra of the C=O stretching region for phenyl acetic acid (PAA) in the liquid state at temperatures 363, 393, 433 and 473 K.

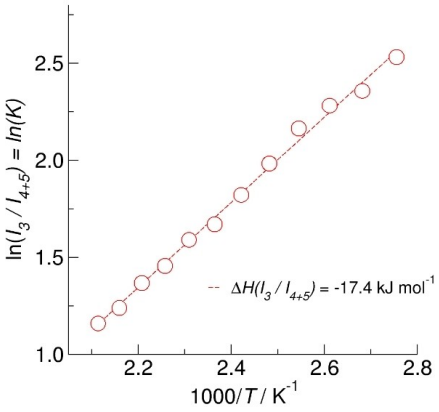

Figure 8. Plots of the natural logarithm of the ratios I_3/I_{4+5} versus inverse temperature taken from the deconvoluted spectra of PAA in Figure 6 between 363 and 473 K. The solid lines represent linear fits ($R^2 \geq 0.98$) with slopes indicating the transfer enthalpies.

transition enthalpy is almost 10 kJ mol^{-1} lower. Thus, there is more energy required to break the HBs in the cyclic dimers in the molecular compared to the ionic system with ions of like charge. Obviously, there is still substantial repulsive Coulomb forces in the IL cationic dimer in the order of half a typical HB energy. In future studies it will be interesting to see whether and to which extend the transition enthalpies of the cationic dimers will change with increasing alkyl chain length between the COOH and the cation in the series of [HOOC-$(CH_2)_n$-py][NTf_2] with $n > 1$. Do they finally reach the values of the molecular systems such as phenyl-acetic acid (HOOC-CH_2-Ph) or phenyl-propanoic acid (HOOC-CH_2-CH_2-Ph) compared to the results presented here?

The gas phase: Vaporization enthalpy predicted from "centerpiece" method

The standard molar enthalpies of vaporization, $\Delta_l^g H_m^o$, of ionic liquids are essential for quantifying intermolecular interactions. The experimental determination of enthalpy of vaporization is a challenging task, so the experimental values must be validated with every theoretical method. A general approach to estimating enthalpies of vaporization based on a so-called "centerpiece" molecule is under development in our recent work.[65,66] This approach is related to the conventional group additivity (GA), where the property of a molecule of interest is collected from a set of possibly small groups with well-defined contributions.[67] In contrast, the idea of the "centerpiece" approach is to select a potentially large "core" molecule that can mimic the structure of the molecule of interest, but the selected "core" molecule is supposed to possess well-established thermodynamic properties.[65,66] For example, the [CH_3-CH_2-py][NTf_2] can be considered as the "centerpiece" molecules to predict vaporization enthalpy of the similarly shaped COOH-substituted ionic liquid [HOOC-(CH_2)-py][NTf_2] as it shown in Figure 9. First of all, the reliable experimental enthalpy of vaporization $\Delta_l^g H_m^o(298.15\ K) = 131.7 \pm 1.4$ kJ mol^{-1} of [CH_3-CH_2-py][NTf_2] was measured in our laboratory using the quartz-crystal microbalance and it was shown to be consistent with data available for the alkyl-pyridinium based ionic liquids with the C_2 to C_8 chain length.[68]

It is quite obvious, that [CH_3-CH_2-py][NTf_2] as the "centerpiece" molecule already contains all essential energetic contributions to the enthalpy of vaporization due to the van der Waals and Coulomb interactions in the liquid phase. Such a specific sum of contributions is unique to the [CH_3-CH_2-py][NTf_2] as the "centerpiece" molecule and hardly can be represented by

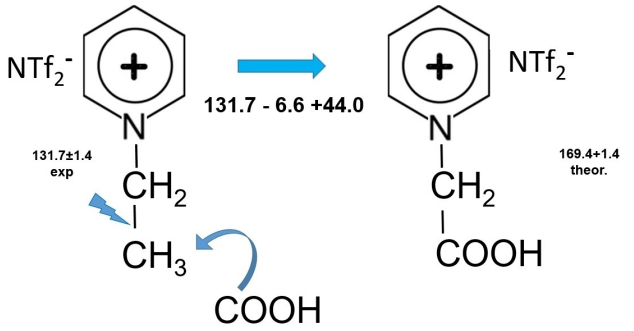

Figure 9. Algorithm for calculating vaporization enthalpies of COOH-containing ILs presented for the example of 1-(carboxymethyl)pyridinium bis(trifluoromethylsulfonyl)imide [HOOC-CH_2-py][NTf_2].

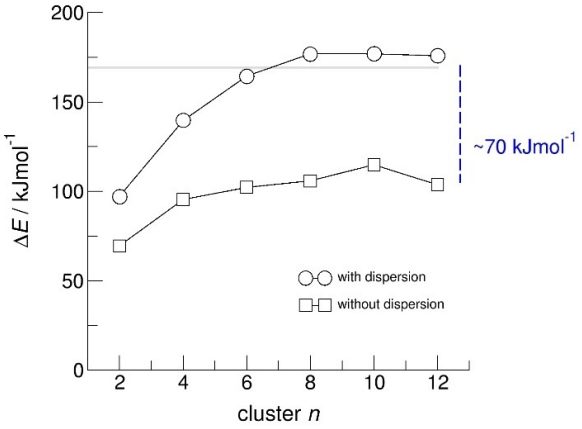

Figure 10. Binding energies ΔE per ion pair (c^+–a^-) for multiples of the clusters (c^+=c^+)(a^-)$_2$ (n = 2) representing constituents of the ionic liquids [HOOC-CH_2-py][NTf_2] calculated at the B3LYP/6-31G* (□) and B3LYP–D3/6-31G* (○) levels of theory. The gray bar indicates the predicted vaporization enthalpy of the IL. The error bar for the calculated energies is about ±5 kJ mol^{-1}.

any other method. This special feature of the "centerpiece" approach significantly increases the reliability of the vaporization enthalpy prediction for the similarly shaped molecules, for example, for [HOOC-CH_2-py][NTf_2] or for the ILs with the longer alkyl chain between the pyridinium ring and carboxyl group.

It is obvious from the algorithm shown in Figure 9, that in order to "construct" the molecule [HOOC-CH_2-py][NTf_2] from the "centerpiece" [CH_3-CH_2-py][NTf_2] we need only to cut the CH_3-fragment and to attach the COOH-group instead. The contributions for $\Delta_l^g H_m^o(CH_3) = 6.33$ kJ mol^{-1} and $\Delta_l^g H_m^o(COOH) = 44.0$ kJ mol^{-1} are well-established for the *molecular* liquids.[69,70] The principle transferability of the $\Delta_l^g H_m^o(R)$ contributions from *molecular liquids* to *ionic liquids* was explored and validated in our recent work.[65,66] Thus, the numerical value for the vaporization enthalpy of [HOOC-CH_2-py][NTf_2] was calculated as follows: $\Delta_l^g H_m^o(298.15\ K) = (131.7 - 6.33 + 44.0)$ kJ mol^{-1} = 169.4 kJ mol^{-1} (Figure 9).

DFT calculations of (c^+=c^+)(a^-)$_2$, (c^+–c^+–a^-)(a^-) (c^+–a^-)$_2$ hydrogen bonded complexes

For validation of the predicted enthalpy of vaporization derived from the above described "centerpiece" method, we calculated clusters of the IL up to 12 "ion pairs" (n = 12) at the B3LYP–D3/6-31G* level of theory considering Grimme's D3-dispersion correction.[51–53] We could show earlier that such a cluster size is sufficient to reproduce liquid-phase properties.[54–57] As shown in Figure 3 we firstly calculated the interaction energies of clusters [(c^+=c^+)(a^-)^2]$_{n/2}$ with n = 2, 4, 6, 8, 10, and 12 relative to the energy of an isolated ion pair (c^+–a^-), which is supposed to be the present species in the gas phase. Unfortunately, we were not able to calculate the frequencies and thus the thermal enthalpies for the largest clusters (n > 6). For this reason, we related the calculated energy differences for the various sized clusters to the measured vaporization enthalpies. Indeed, for larger cluster sizes (n > 6) the calculated value for the PIL converges to the predicted vaporization enthalpy of about 169.4 kJ mol^{-1} as shown in Figure 10. Calculating all clusters without taking additional dispersion interaction into account, the vaporization enthalpies of the APILs (aprotic ionic liquids) is about 70 kJ mol^{-1} lower than the "centerpiece" value, showing that dispersion forces need to be included for comparison with data derived from experiment. Additionally, we calculated the interaction energies of complexes [(c^+–c^+–a^-)(a^-)]$_{n/2}$ with n = 2, 4, 6, 8, 10, and 12 relative to the energy of an isolated ion pair ($c^+ = -a^-$). This has been done because we know from our IR measurements that both, (c^+=c^+)(a^-)^2 and (c^+–c^+–a^-)(a^-) complexes are present in the liquid phase before vaporization into the gas phase as isolated ion pairs (c^+–a^-). In Figure 11, we show that that the energy differences to the isolated ion pairs converge to a somewhat lower value than for the (c^+=c^+)(a^-)^2 species. Despite assumptions and inaccuracies of the chosen approach, the energy differences for the large (c^+=c^+)(a^-)^2 and (c^+–c^+–a^-)(a^-) complexes with n = 10, 12 are surprisingly close

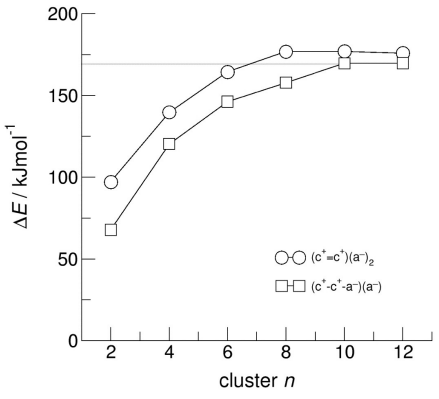

Figure 11. Binding energies ΔE per ion pair (c^+–a^-) for multiples of the clusters (c^+=c^+)(a^-)$_2$ (○) and (c^+–c^+–a^-)(a^-) (n = 2; □) representing constituents of the ionic liquids [HOOC-CH_2-py][NTf_2] calculated at the B3LYP–D3/6-31G* level of theory. The gray bar indicates the predicted vaporization enthalpy of the IL. The error bar for the calculated energies is about ±5 kJ mol^{-1}.

to the transfer enthalpy of about $-8\,kJ\,mol^{-1}$ derived from the IR spectra within the liquid phase. Thus, the calculated energies for both type of complexes support the order of transfer enthalpies derived from IR measurements and thermodynamic methods.

Conclusions

We have shown that the carboxyl-functionalized ionic liquid 1-(carboxymethyl)pyridinium bis(trifluoromethylsulfonyl)imide [HOOC-CH_2-py][NTf_2] exhibits three types of hydrogen bonding. We observed doubly hydrogen bonded cationic dimers ($c^+{=}c^+$) in the X-ray patterns of the crystalline state. Despite the repulsive Coulomb forces among the cations, only the doubly hydrogen bonding motif between the carboxyl groups is present. Upon melting, this binding motif opens and is replaced by ($c^+{-}c^+{-}a^-$) species, with a remaining single cationic hydrogen bond and an additional hydrogen bond between cation and anion. IR measurements in the bulk liquid phase over a large temperature range allowed a transition enthalpy of about $-8\,kJ\,mol^{-1}$ to be determined. This is less than half of the resulting transfer enthalpy of the molecular mimic of the APIL cation, phenyl acetic acid, derived by the same approach. The difference can be referred to the repulsive Coulomb interaction between the cations, which allows the doubly hydrogen bonded motif to be broken with significantly less energy. Moreover, we predicted the vaporization enthalpy of the carboxyl-functionalized ionic liquid 1-(carboxymethyl)pyridinium bis(trifluoromethylsulfonyl)imide [HOOC-CH_2-py][NTf_2] by using the "centerpiece" method based on reliably measured vaporization enthalpies and relating vaporization energetics of *molecular* liquids to those of *ionic* liquids. The obtained value of about $169.4\,kJ\,mol^{-1}$ could be confirmed by DFT calculated energies of differently sized $(c^+{=}c^+)(a^-)^2$ and ($c^+{-}c^+{-}a^-$)(a^-) complexes related to the gas-phase ion pairs ($c^+{-}a^-$). This agreement also justifies the assumption that the ionic liquid evaporates as hydrogen-bonded ion pairs ($c^+{-}a^-$) into the gas phase. The measured transition enthalpies allow the noncovalent interaction to be dissected and the strength of hydrogen bonds between ions of like charge to be determined. Herein, we have demonstrated that combining X-ray crystallography, differential scanning calorimetry, IR spectroscopy, thermodynamic methods and DFT calculations allows the analysis and characterization of all types of hydrogen bonding present in the solid, liquid and gaseous states of ionic liquids. In particular, this work shows that structure and thermodynamics result from a delicate balance of intermolecular forces, depending on whether those are long or short range.

Acknowledgements

R.L. and S.P.V. acknowledge financial support from German Science Foundation (DFG) within the frame of the priority program SPP 1807 SPP 1807 "*Control of London Dispersion Interactions in Molecular Chemistry*", grant LU-506/12-2 to R.L. and grant VE 265-9/2 to S.P.V. This work was also supported by DFG Research Grants LU-506/14-2, project no. 286149019 and LU-506/17-1, project no. 470038970. Open Access funding enabled and organized by Projekt DEAL.

Conflict of Interest

The authors declare no conflict of interest.

Keywords: density functional calculations · hydrogen bonds · IR spectroscopy · noncovalent interactions · X-ray diffraction

[1] H. Weingärtner, *Angew. Chem. Int. Ed.* **2008**, *47*, 654–670; *Angew. Chem.* **2008**, *120*, 664–682; *Angew. Chem.* **2008**, *120*, 664–682; *Angew. Chem. Int. Ed.* **2008**, *47*, 654–670.
[2] F. Endres, S. Z. El Abedin, *Phys. Chem. Chem. Phys.* **2006**, *8*, 2101–2116.
[3] T. Welton, *Chem. Rev.* **1999**, *99*, 2077–2084.
[4] N. V. Plechkova, K. R. Seddon, *Chem. Soc. Rev.* **2008**, *37*, 123–150.
[5] S. P. M. Ventura, F. A. e Silva, M. V. Quental, D. Mondal, M. G. Freire, J. A. P. Coutinho, *Chem. Rev.* **2017**, *117*, 6984–7052.
[6] D. R. MacFarlane, N. Tachikawa, M. Forsyth, J. M. Pringle, P. C. Howlett, G. D. Elliott, J. H. Davis, Jr., M. Watanabe, P. Simon, C. A. Angell, *Energy Environ. Sci.* **2014**, *7*, 232–250.
[7] M. Galiński, A. Lewandowski, I. Stępniak, *Electrochim. Acta.* **2006**, *51*, 5567–5580.
[8] S. Mennea, J. Piresb, M. Anoutib, A. Balducci, *Electrochem. Commun.* **2013**, *31*, 39–41.
[9] K. Fumino, R. Ludwig, *J. Mol. Liq.* **2014**, *192*, 94–102.
[10] K. Fumino, S. Reimann, R. Ludwig, *Phys. Chem. Chem. Phys.* **2014**, *40*, 21903–21929.
[11] K. Fumino, A. Wulf, R. Ludwig, *Angew. Chem. Int. Ed.* **2008**, *47*, 8731–8734; *Angew. Chem.* **2008**, *120*, 8859–8862.
[12] K. Fumino, T. Peppel, M. Geppert-Rybczyńska, D. H. Zaitsau, J. K. Lehmann, S. P. Verevkin, M. Köckerling, R. Ludwig, *Phys. Chem. Chem. Phys.* **2011**, *13*, 14064–14075.
[13] P. A. Hunt, C. R. Ashworth, R. P. Matthews, *Chem. Soc. Rev.* **2015**, *44*, 1257–1288.
[14] C. R. Ashworth, R. P. Matthews, T. Welton, P. A. Hunt, *Phys. Chem. Chem. Phys.* **2016**, *18*, 18145–18160.
[15] F. N. Keutsch, R. J. Saykally, *Proc. Natl. Acad. Sci. USA* **2001**, *98*, 10533–10540.
[16] R. Ludwig, *Angew. Chem. Int. Ed.* **2001**, *40*, 1808–1827; *Angew. Chem.* **2001**, *113*, 1856–1876.
[17] F. Huisken, M. Stemmler, *Chem. Phys. Lett.* **1988**, *144*, 391–395.
[18] H. L. Han, C. Camacho, H. A. Witek, Y. P. Lee, *J. Chem. Phys.* **2011**, *134*, 144309.
[19] A. Knorr, K. Fumino, A.-M. Bonsa, R. Ludwig, *Phys. Chem. Chem. Phys.* **2015**, *17*, 30978–30982.
[20] A. Knorr, R. Ludwig, *Sci. Rep.* **2015**, *5*, 17505.
[21] A. Knorr, P. Stange, K. Fumino, F. Weinhold, R. Ludwig, *ChemPhysChem* **2016**, *17*, 458–462.
[22] A. Strate, T. Niemann, D. Michalik, R. Ludwig, *Angew. Chem. Int. Ed.* **2017**, *56*, 496–500; *Angew. Chem.* **2017**, *129*, 510–514.
[23] T. Niemann, D. H. Zaitsau, A. Strate, A. Villinger, R. Ludwig, *Sci. Rep.* **2018**, *8*, 14753.
[24] A. Strate, V. Overbeck, V. Lehde, J. Neumann, A.-M. Bonsa, T. Niemann, D. Paschek, D. Michalik, R. Ludwig, *Phys. Chem. Chem. Phys.* **2018**, *20*, 5617–5625.
[25] T. Niemann, J. Neumann, P. Stange, S. Gärtner, T. G. A. Youngs, D. Paschek, G. G. Warr, R. Atkin, R. Ludwig, *Angew. Chem. Int. Ed.* **2019**, *58*, 12887–12892; *Angew. Chem.* **2019**, *131*, 13019–13024.
[26] A. E. Khudozhitkov, V. Overbeck, P. Stange, D. Paschek, A. G. Stepanov, D. I. Kolokolov, R. Ludwig, *Angew. Chem. Int. Ed.* **2019**, *58*, 17863–17871; *Angew. Chem.* **2019**, *131*, 18027–18035.
[27] A. E. Khudozhitkov, T. Niemann, P. Stange, M. Donoshita, A. G. Stepanov, H. Kitagawa, D. I. Kolokolov, R. Ludwig, *J. Phys. Chem. Lett.* **2020**, *11*, 6000–6006.

[28] A. Strate, J. Neumann, T. Niemann, P. Stange, A. E. Khudozhitkov, A. G. Stepanov, D. Paschek, D. I. Kolokolov, R. Ludwig, *Phys. Chem. Chem. Phys.* **2020**, *22*, 6861–6867.
[29] J. Neumann, D. Paschek, R. Ludwig, *J. Phys. Chem. B* **2021**, *125*, 1, 281–286.
[30] J. Neumann, R. Ludwig, D. Paschek, *J. Phys. Chem. B* **2021**, *125*, 19, 5132–5144.
[31] H. Li, T. Niemann, R. Ludwig, R. Atkin, *J. Phys. Chem. Lett.* **2020**, *11*, 3905–3910.
[32] T. Niemann, D. H. Zaitsau, A. Strate, P. Stange, R. Ludwig, *Phys. Chem. Chem. Phys.* **2020**, *22*, 2763–2774.
[33] F. S. Menges, H. J. Zeng, P. J. Kelleher, O. Gorlova, M. A. Johnson, T. Niemann, A. Strate, R. Ludwig, *J. Phys. Chem. Lett.* **2018**, *9*, 2979–2984.
[34] T. Niemann, A. Strate, R. Ludwig, H. J. Zeng, F. S. Menges, M. A. Johnson, *Angew. Chem. Int. Ed.* **2018**, *57*, 15364–15368.
[35] T. Niemann, A. Strate, R. Ludwig, H. J. Zeng, F. S. Menges, M. A. Johnson, *Phys. Chem. Chem. Phys.* **2019**, *21*, 18092–18098.
[36] H. J. Zeng, F. S. Menges, T. Niemann, A. Strate, R. Ludwig, M. A. Johnson, *J. Phys. Chem. Lett.* **2020**, *11*, 683–688.
[37] A. Strate, T. Niemann, R. Ludwig, *Phys. Chem. Chem. Phys.* **2017**, *19*, 18854–18862.
[38] T. Niemann, P. Stange, A. Strate, R. Ludwig, *ChemPhysChem* **2018**, *19*, 1691–1695.
[39] T. Niemann, P. Stange, A. Strate, R. Ludwig, *Phys. Chem. Chem. Phys.* **2019**, *21*, 8215–8220.
[40] J. K. Philipp, S. Fritsch, R. Ludwig, *ChemPhysChem* **2020**, *21*, 2411–2416.
[41] J. K. Philipp, R. Ludwig, *Molecules* **2020**, *25*, 4972.
[42] a) F. Weinhold, R. A. Klein, *Angew. Chem. Int. Ed.* **2014**, *53*, 11214–11217; b) F. Weinhold, R. A. Klein, *Angew. Chem. Int. Ed.* **2014**, *53*, 12992; c) G. Frenking, G. F. Camamori, *Angew. Chem. Int. Ed.* **2015**, 54, 2596–2599.
[43] F. Weinhold, *Angew. Chem. Int. Ed.* **2017**, *56*, 14577–14581.
[44] F. Weinhold, *Inorg. Chem.* **2018**, *57*, 2035–2044.
[45] I. Mata, I. Alkorta, E. Molins, E. Espinosa, *ChemPhysChem* **2012**, *13*, 1421–1424.
[46] P. Nockemann, B. Thijs, T. N. Parac-Vogt, K. Van Hecke, L. Van Meervelt, B. Tinant, I. Hartenbach, T. Schleid, V. Thi Ngan, M. T. Nguyen, K. Binnemans, *Inorg. Chem.* **2008**, *47*, 9987–9999.
[47] a) G. M. Sheldrick, *Acta Crystallogr. Sect. A* **2008**, *64*, 112–122; b) G. M. Sheldrick, *Acta Crystallogr. Sect. C* **2015**, *71*, 3–8.
[48] L. Krause, R. Herbst-Irmer, G. M. Sheldrick, D. Stalke, *J. Appl. Crystallogr.* **2015**, *48*, 3–10.
[49] L. Al Sheakh, T. Niemann, A. Villinger, P. Stange, D. Zaitsau, A. Strate, R. Ludwig, *ChemPhysChem* **2021**, *22*, 1850–1856.
[50] *Gaussian 09, Revision D.01*, M. J. Frisch, G. W. Trucks, H. B. Schlegel, G. E. Scuseria, M. A. Robb, J. R. Cheeseman, G. Scalmani, V. Barone, G. A. Petersson, H. Nakatsuji, X. Li, M. Caricato, A. Marenich, J. Bloino, B. G. Janesko, R. Gomperts, B. Mennucci, H. P. Hratchian, J. V. Ortiz, A. F. Izmaylov, J. L. Sonnenberg, D. Williams-Young, F. Ding, F. Lipparini, F. Egidi, J. Goings, B. Peng, A. Petrone, T. Henderson, D. Ranasinghe, V. G. Zakrzewski, J. Gao, N. Rega, G. Zheng, W. Liang, M. Hada, M. Ehara, K. Toyota, R. Fukuda, J. Hasegawa, M. Ishida, T. Nakajima, Y. Honda, O. Kitao, H. Nakai, T. Vreven, K. Throssell, J. A. Montgomery, Jr., J. E. Peralta, F. Ogliaro, M. Bearpark, J. J. Heyd, E. Brothers, K. N. Kudin, V. N. Staroverov, T. Keith, R. Kobayashi, J. Normand, K. Raghavachari, A. Rendell, J. C. Burant, S. S. Iyengar, J. Tomasi, M. Cossi, J. M. Millam, M. Klene, C. Adamo, R. Cammi, J. W. Ochterski, R. L. Martin, K. Morokuma, O. Farkas, J. B. Foresman, D. J. Fox, Gaussian, Inc., Wallingford CT, **2013**.
[51] S. Grimme, J. Antony, S. Ehrlich, H. Krieg, *J. Chem. Phys.* **2010**, *132*, 154104.
[52] S. Ehrlich, J. Moellmann, W. Reckien, T. Bredow, S. Grimme, *ChemPhysChem.* **2011**, *12*, 3414–3420.
[53] S. Grimme, A. Jansen, *Chem. Rev.* **2016**, *116*, 5105–5154.
[54] R. Ludwig, *ChemPhysChem* **2000**, *1*, 53–56.
[55] R. Ludwig, F. Weinhold, T. C. Farrar, *J. Chem. Phys.* **1995**, *103*, 6941–6950.
[56] R. Ludwig, *ChemPhysChem.* **2005**, *6*, 1369–1375.
[57] V. N. Emel'yanenko, P. Stange, J. Feder-Kubis, S. P. Verevkin, R. Ludwig, *Phys. Chem. Chem. Phys.* **2020**, *22*, 4896 4904.
[58] S. F. Boys, F. Bernardi, *Mol. Phys.* **1970**, *19*, 553–566.
[59] L. M. Mentel, E. J. Baerends, *J. Chem. Theory Comput.* **2014**, *10*, 252–267.
[60] E. Perlt, M. von Domaros, B. Kirchner, R. Ludwig, F. Weinhold, *Sci. Rep.* **2017**, *7*, 10244.
[61] S. P. Verevkin, K. V. Zherikova, E. A. Martynenko, *J. Mol. Liq.* **2022**, *350*, 118576.
[62] R. Kalescky, E. Kraka, D. Cremer, *J. Chem. Phys.* **2014**, *140*, 084315.
[63] F. Kollipost, R. W. Larsen, A. V. Domanskaya, M. Nörenberg, M. A. Suhm, *J. Chem. Phys.* **2012**, *136*, 151101.
[64] Z. Xue, M. A. Suhm, *Mol. Phys.* **2010**, *108*, 2279–2288.
[65] S. P. Verevkin, K. V. Zherikova, E. A. Martynenko, *J. Mol. Liq.* **2022**, *350*, 118576.
[66] S. P. Verevkin, D. H. Zaitsau, R. Ludwig, *Molecules* **2022**, *27*, 2321.
[67] S. P. Verevkin, V. N. Emel'yanenko, V. Diky, C. D. Muzny, R. D. Chirico, M. Frenkel, *J. Phys. Chem. Ref. Data* **2013**, 42, 033102.
[68] D. H. Zaitsau, A. V. Yermalayeu, V. N. Emel'yanenko, S. P. Verevkin, U. Welz-Biermann, T. Schubert, *Sci. China Chem.* **2021**, *55*, 1525–1531.
[69] M. Ducros, J. F. Gruson, H. Sannier, *Thermochim. Acta* **1980**, *36*, 39–65.
[70] S. P. Verevkin, S. Kondratev, D. Zaitsau, K. Zherikova, R. Ludwig, *J. Mol. Liq.* **2021**, *343*, 117547.

Manuscript received: March 28, 2022
Accepted manuscript online: July 3, 2022
Version of record online: July 13, 2022